Pramāṇa, Vol. 23, No. 5, November 1984, pp. 573–593. © Printed in India.

Infrared studies on ion irradiated quartz

A K SOOD*, V UMADEVI**, R KESAVAMOORTHY and G VENKATARAMAN

Reactor Research Centre, Kalpakkam 603 102, India
* Present address: Max-Planck-Institut fur Festkorperforschung, Heisenberg Strasse 1, 7000 Stuttgart 80, Federal Republic of Germany
** Present address: Department of Physics, University of Missouri, Columbia, Missouri 65211, USA

MS received 29 March 1984; revised 23 July 1984

Abstract. Damage produced in α- and fused quartz bombarded with low energy (~ 100 keV) D^+, He^+ and Ar^+ ions, has been studied by observing the changes in the IR spectrum. Besides bulk reflectivity, the attenuated total reflection spectrum has also been studied, the latter with a view to obtaining the surface polariton frequencies. It is observed that for the same fluence, the changes following D^+ irradiation are much higher compared to that for Ar^+ irradiation. The variation of the surface polariton frequency in α-quartz with the damage energy deposited has the same trend as observed earlier for refractive index. Some annealing studies have also been performed in argon-irradiated samples. These studies indicate that whereas in fused quartz the damaged layer recovers completely, in α-quartz there is a residual amorphization even after annealing. A two-layer model is proposed which gives a reasonable simulation of the observed IR properties.

Keywords. Infrared reflectivity; ion-irradiation; annealing; quartz; surface polariton; Kramer-Kronig analysis.

PACS No. 78·30 Gt, 60·80 Jh

1. Introduction

Irradiation effects have been extensively studied in fused and α-quartz, the two well-known modifications of SiO_2. It has been shown (Hines and Arndt 1960; Schineller *et al* 1968; Bayly 1973; Presby and Brown 1976; Karge and Prager 1976; Webb and Townsend 1976) that the refractive index n (in the visible range) of α-quartz decreases on ion bombardment whereas it increases in fused quartz (FQ). This behaviour is illustrated in figure 1 taken from the work of Gotz (1981).

In their pioneering work on radiation compaction, Primak and co-workers (Primak and Kampwirth 1968; Primak 1975, 1976) showed that the density of α-quartz decreases on irradiation, saturating with dose at a value for the density which is about 15 % smaller than that for the unirradiated material. The effect in FQ is opposite but the net changes are small, the total increase in density being about 2–3 %. The changes in refractive index alluded to the above have been correlated with radiation-induced density changes (Brueckner 1971; Revesz 1972), and Revesz (1972) has in particular proposed that the changes in vitreous silica are connected with a modification of the SiO_4 tetrahedron network.

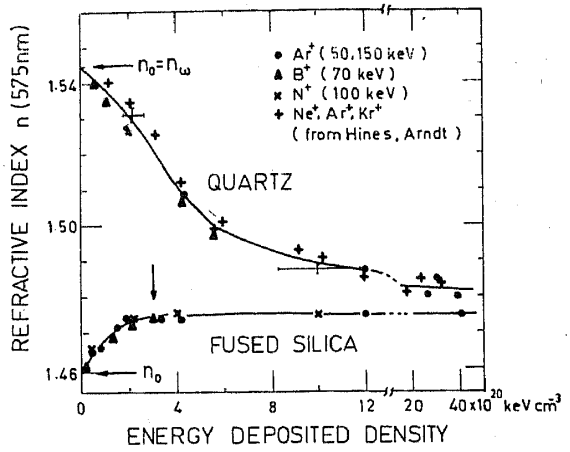

Figure 1. Variation of refractive index of α-quartz and FQ following ion bombardment, as a function of energy deposited density (after Gotz 1981).

The effects produced by neutron bombardment in α-quartz and FQ have been studied by a variety of techniques like Raman and IR spectroscopy, small-angle x-ray scattering and electron microscopy (Bates *et al* 1974; Gaskell and Johnson 1976; Grasse *et al* 1981) and it has been observed that at a fluence of $\sim 2 \times 10^{20}$ neutrons/cm^2, the α-quartz sample transformed essentially to a noncrystalline material (Bates *et al* 1974).

In this paper we address ourselves to a detailed IR study of α- and fused quartz subjected to ion bombardment. Such a study is also of practical interest since quartz is finding increasing use in optoelectronic devices. Ion bombardment is often a part of the materials processing in device technology, and one would like to have some assessment of the possible damage. Besides bulk reflectivity (BR), we have also studied the attenuated total reflection (ATR), both in the spectral range 4000–180 cm^{-1}. The latter technique, gives information about surface polaritons (Otto 1968). It is to be noted that while IR results for neutron irradiated quartz exist (Gaskell and Johnson 1976), similar results are not available for quartz subjected to ion bombardment, and this in fact was the motivation for the present experiments. While this work was in progress (Umadevi *et al* 1979, 1980), a report appeared due to Zhizhin *et al* (1979) wherein the effect of bombardment by 100 and 200 keV nitrogen ions on the bulk reflectivity and one of the surface polaritons of α-quartz was described.

In our work, we have subjected the samples to bombardment by 100 keV deuterium, helium and argon ions. Besides carrying out post irradiation BR and ATR measurements, we have also performed several annealing studies. Especially in the case of D^+ irradiation, the doses were chosen so as to span a substantial portion of the range of deposited energy density of figure 1.

The experimental details are described in §2. The calculated damage profiles corresponding to the irradiation conditions are given in §3. The experimental results are summarized in §4 in the following sequence: (i) Bulk reflectivity of α-quartz irradiated with D^+, He^+ and Ar^+ ions, (ii) surface polaritons in irradiated α-quartz, (iii) annealing results for α-quartz irradiated with Ar^+ ions, (iv) BR and ATR spectra for irradiated fused quartz and annealing results for fused quartz irradiated with Ar^+. The analysis of the data is discussed in §5. Besides presenting a conventional Kramer-Kronig analysis, a model for understanding our results is also considered. A two-layer model with the top layer representing the damaged material and the bottom one the

undamaged material, gives a reasonable simulation of the observed IR properties. The summary and conclusions are given in §6. The expressions for the calculation of surface polariton spectra are consigned to an appendix.

2. Experimental details

Single crystals of (natural) α-quartz (of Optical Engineering Lab, Masulipatnam) in the form of polished slabs (size 15 × 15 × 1 mm) cut parallel to the optic axis were used. FQ of spectral grade (or Thermal Syndicate Limited UK) (of Spectra System, Bangalore) in the form of optically polished discs (size: 12 mm dia × 2 mm thick) were used. The samples were checked for impurities using atomic absorption spectroscopy and x-ray fluorescence, and the impurity levels were < 50 ppm.

All irradiations (Sames J-15, 150 keV ion accelerator) were performed at room temperature with deuterium, helium and argon ions of (nominal) energy of 100 keV. The specimens were mounted in a target chamber maintained at a vacuum of $\sim 2 \times 10^{-6}$ torr during irradiation. The ion beam current was kept less than 2 μA/cm^2 ($\sim 1{\cdot}3 \times 10^{13}$ ions/cm^2 sec) for most of the irradiations. Only one sample, namely Q5 (see table 1) was irradiated at a higher current density (15 μA/cm^2). The samples were attached to the copper target holder by silver paint. Silver paint was also applied to the edges of the top surface and sides of the sample to provide a conducting path for the accumulated charge. The experimental set up used for irradiation is described in detail elsewhere (Nandedkar 1981).

The ion beam was incident normal to the sample surface. The sample holder was surrounded by a copper shield cooled to liquid nitrogen temperature in order to minimize the deposition of free carbon liberated during the cracking of pump oil vapour during irradiation. Notwithstanding this, the irradiated samples were subsequently maintained at 300°C for 1 hr in an oxygen atmosphere to remove any possible carbon deposit ($\lesssim 50$ Å) that might have formed. We have reasons to believe that this processing did not cause any substantial alteration to the properties of the irradiated specimen.

The irradiation dose was estimated by measuring the charge, after suitably suppressing the contribution from secondary electron emission. The irradiation details are summarized in table 1 along with some particulars about damage profiles (to be discussed in §3).

As remarked in §1, some annealing studies were also carried out. To reach the annealing temperature, a heating rate of ~ 25°C/min was usually employed. On reaching the desired temperature, the furnace was adjusted to hold the temperature constant (to within ± 2°C). After annealing for 1 hr, the sample was brought back to room temperature for spectroscopic investigations. The cooling rate employed was similar to the heating rate. In the region 500–600°C, the heating and cooling rates employed were much lower, being of the order of ~ 3°C/min. This was to prevent the cracking of α-quartz at the α-β transition.

All IR spectra, both BR and ATR, were recorded at room temperature (Perkin-Elmer model 580 spectrophotometer) in the range 4000–180 cm^{-1}. For the BR measurements, the average angle of incidence was $\sim 10°$ from the normal to the sample surface. By suitably selecting the polarization of the IR beam, either the E or the A_2 modes of

Table 1. Irradiation parameters.

Sample number	Incident ion	Fluence (ion/cm^2)	$S^{max}(x) \times$ fluence (keV/cm^3)
α-Quartz			
Q1	D^+	2×10^{14}	$7{\cdot}2 \times 10^{18}$
Q2	D^+	4×10^{15}	$1{\cdot}4 \times 10^{20}$
Q3	D^+	8×10^{15}	$2{\cdot}9 \times 10^{20}$
Q4	D^+	$2{\cdot}6 \times 10^{16}$	$9{\cdot}4 \times 10^{20}$
Q5	D^+	$9{\cdot}9 \times 10^{16}$	$3{\cdot}6 \times 10^{21}$
Q6	He^+	$2{\cdot}5 \times 10^{16}$	$4{\cdot}9 \times 10^{21}$
Q7	Ar^+	4×10^{15}	$2{\cdot}5 \times 10^{22}$
Q8	Ar^+	5×10^{16}	$3{\cdot}1 \times 10^{23}$
Fused Quartz			
FQ10	D^+	2×10^{14}	$6{\cdot}6 \times 10^{18}$
FQ11	D^+	4×10^{15}	$1{\cdot}3 \times 10^{20}$
FQ12	D^+	$2{\cdot}6 \times 10^{16}$	$8{\cdot}6 \times 10^{20}$
FQ13	He^+	$2{\cdot}5 \times 10^{16}$	$4{\cdot}2 \times 10^{21}$
FQ14	Ar^+	1×10^{15}	$5{\cdot}2 \times 10^{21}$
FQ15	Ar^+	1×10^{16}	$5{\cdot}2 \times 10^{22}$

vibration (of α-quartz) could be scanned. In the case of fused quartz, unpolarized spectra were recorded.

The ATR set-up used was a 25-reflection unit, with KRS-5 as the prism. All ATR spectra were recorded at a fixed angle of incidence of 30°. The recorded spectra were suitably corrected for absorption (KRS-5 crystal) to obtain normalized spectra for surface polaritons. Results for ordinary surface polaritons alone are presented.

The BR and ATR spectra were recorded for both sides of the sample prior to irradiation and after irradiation. After annealing treatments also both surfaces were scanned. As is to be expected, the spectra for the unirradiated side remained invariant.

3. Damage profiles

The depth profiles and the profiles for displacement damage energy deposition for 100 keV D^+, He^+ and Ar^+ ions bombarding quartz were calculated using the code E-DEP-1 of Manning and Mueller (1974). The profiles of the damage energy density $S_D(x)$ thus computed are shown in figure 2. The peak energy densities (= fluence $\times S_D^{max}(x)$) achieved in the various irradiations were computed using these profiles and are listed in table 1. It is to be noted that the calculation of $S_D(x)$ does *not* explicitly depend on the structure of quartz *i.e.* whether it is crystalline or amorphous. Only the density of the medium enters the estimation.

Besides computing the damage, we have also estimated the sputtering yield for 100 keV irradiation by the various ions using the theory of Sigmund (1969). The sputtering yield S (in units of atoms/ion) for Ar^+ is $\sim 1{\cdot}25$ which is an order of magnitude higher than that for either D^+ or He^+. As we shall see later, this produces important differences in the post irradiation behaviour.

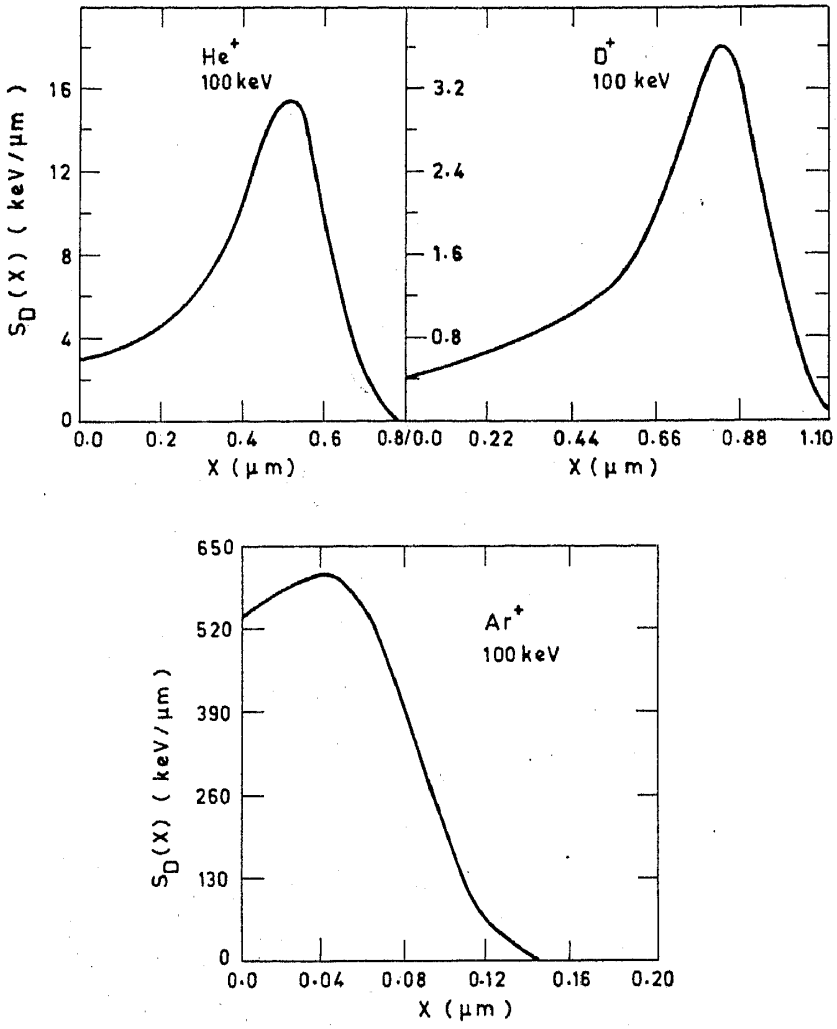

Figure 2. Depth profiles of displacement damage energy deposition for 100 keV D^+, He^+ and Ar^+ ions bombarding quartz, computed using the code of Manning and Mueller (1974).

4. Experimental results

α-quartz belongs to the trigonal class (space group D_3^6) with three formula units per cell. Standard group theoretical analysis shows that there are 24 optic modes, distributed in terms of irreducible representations as: $4A_1(R)$, $4A_2(\text{IR})$ and $8E(\text{IR, R})$. The modes are well studied and their frequencies well known (Scott and Porto 1967). In this work we have confined ourselves to the IR active modes.

4.1 *Bulk reflectivity of α-quartz*

Figure 3 presents typical results for the *E*-mode reflectivity. Additional results for the *E*-mode are given in figure 4 and for the A_2-mode in figure 5. From a scan of the results, the following broad conclusions can be readily drawn: (i) Irradiation leads to an overall reduction in the reflectivity. (ii) The changes in reflectivity are more pronounced following irradiation with D^+ as compared to irradiation with He^+ or Ar^+. Particularly striking is the fact that after deuterium irradiation, the reflection spectrum has strong similarities to that for fused quartz (see figures 4 and 11).

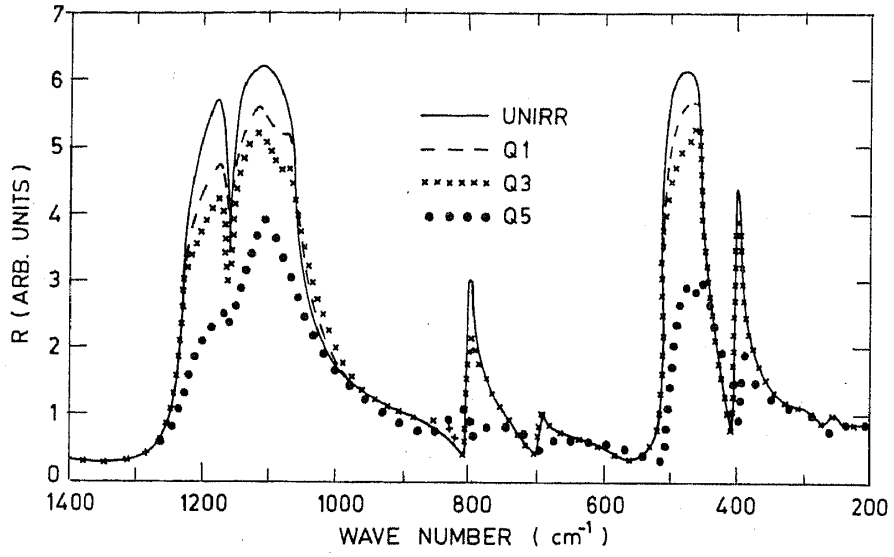

Figure 3. Typical BR spectra for α-quartz in the *E*-mode.

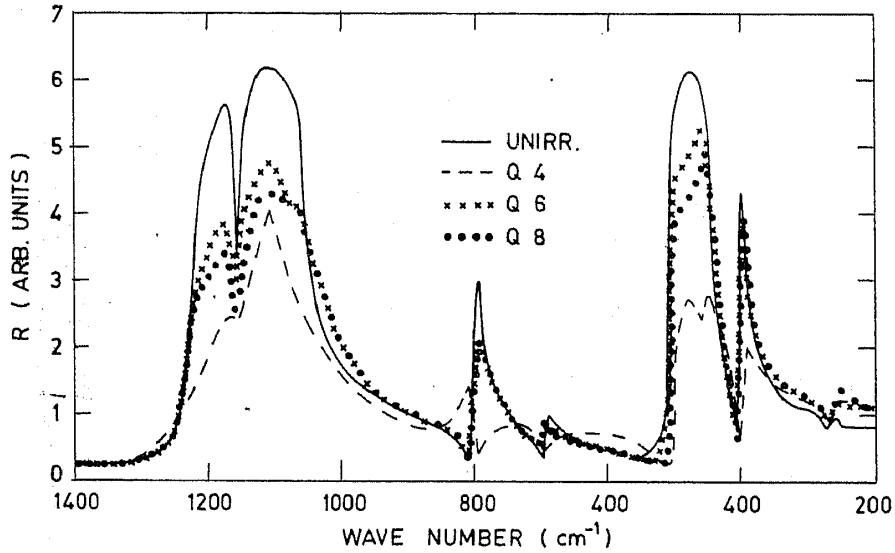

Figure 4. Additional results for α-quartz in the *E*-mode.

There are two reasons for the differences observed between Ar^+ and D^+ irradiations. First, as already noted (§3), the sputtering in argon ion bombardment is much more than in deuterium bombardment; as a result, for the same fluence, less of the dose effects are retained in the former as compared to the latter. Secondly, the ratio of the optical penetration depth to the range of damage is less favourable for Ar^+ than for D^+. Due to a combination of these two effects, the changes in IR spectra are more prominent following deuterium irradiation.

4.2 *Surface polaritons in α-quartz*

ATR spectra for α-quartz in the range 1300–1050 cm^{-1} are shown in figures 6 and 7. These figures are arranged in two groups for clarity as well as convenience. Although

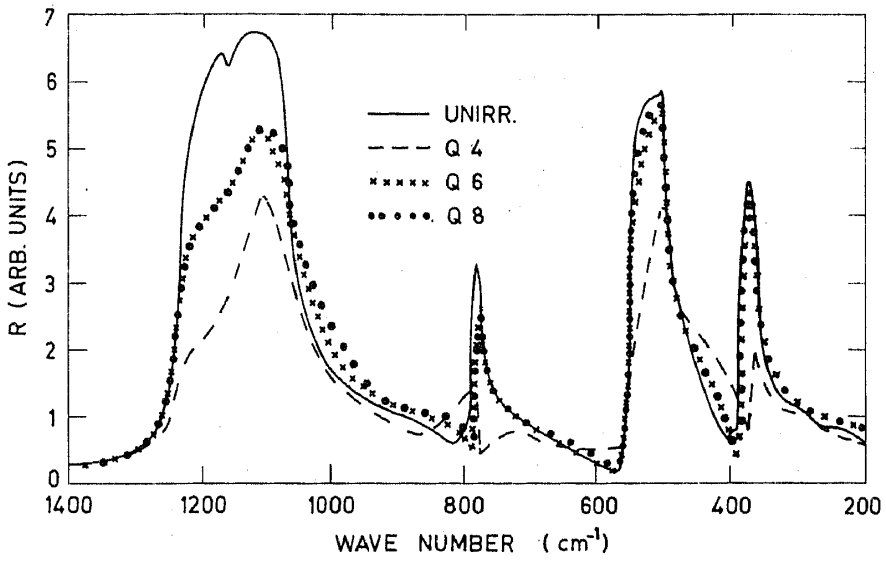

Figure 5. Typical BR spectra for α-quartz in the A_2-mode.

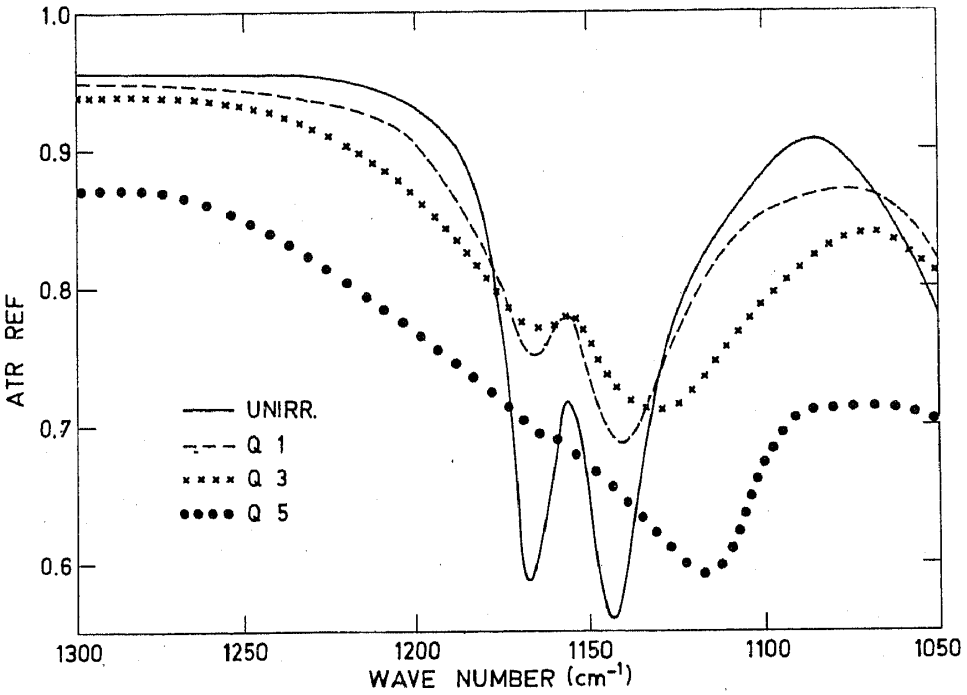

Figure 6. Typical ATR spectra for α-quartz in the range 1300–1050 cm^{-1}.

data are presented for only a limited spectral range, we have scanned the entire range 1400–180 cm^{-1} for the various samples. Of the six ordinary surface polaritons in this range, the two at 1144 cm^{-1} and 487 cm^{-1} shift to lower frequencies by 20 cm^{-1} whereas the remaining four *viz*, those at 1167, 800, 695 and 399 cm^{-1} do not shift significantly. As regards linewidth, it is evident from the data that considerable broadening occurs. Indeed even a line which does not shift (*e.g.* that at 1167 cm^{-1}) shows broadening.

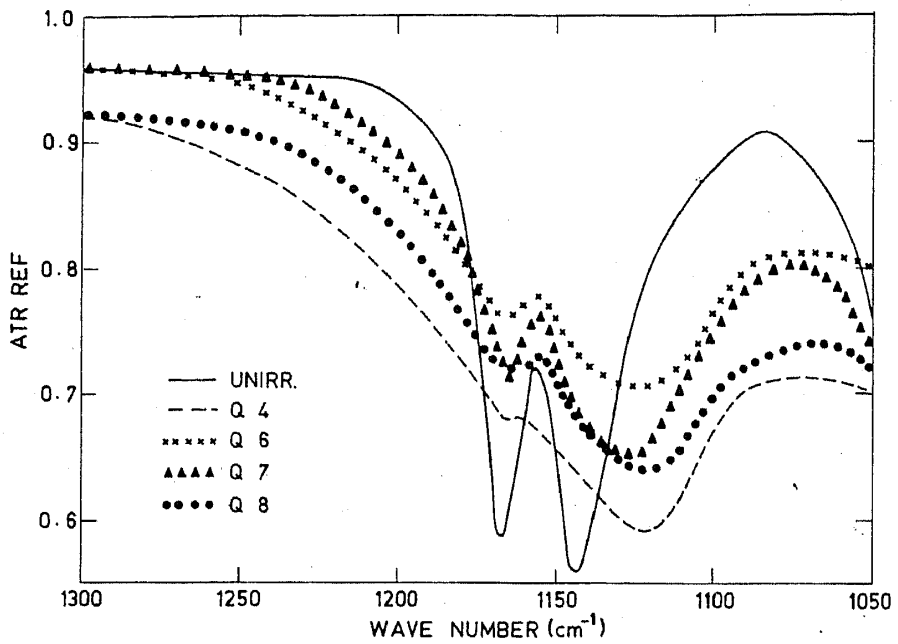

Figure 7. Additional ATR spectra for α-quartz (in the same range as in the previous figure).

Table 2. Frequencies of ordinary surface polaritons in α-quartz.

Sample	Surface polariton frequencies (cm^{-1})						Remarks
Unirradiated	1167	1144	800	695	487	399	Expt.
	1159	1124	800	692	476	401	Calc. (KK)
Q4	1165	1121	795	695	462	399	Expt.
	1156	1110	795	720	475	392	Calc. (KK)
	1160	1125	795	689	456	389	Calc. (Two-layer model $t = 1{\cdot}1$ μm)
Q8	1164	1120	800	695	468	399	Expt.
	1163	1107	800	691	474	401	Calc. (KK)

Unfortunately, there is no unambiguous way of extracting widths from such complex spectra. We content ourselves therefore with reporting the surface polariton frequencies alone, which is given in table 2.

Figure 8 shows the variation of one of the mode frequencies as a function of damage energy deposited following D^+ irradiation. The similarity of trend to that in figure 1 is striking.

4.3 *Ageing and annealing behaviour*

In the course of our work we noticed that a specimen of α-quartz irradiated with argon and left around in the laboratory for several months showed changes in the reflectivity spectrum. Suspecting that some slow annealing was probably taking place at room temperature, we initiated a series of systematic annealing studies. Since no changes with

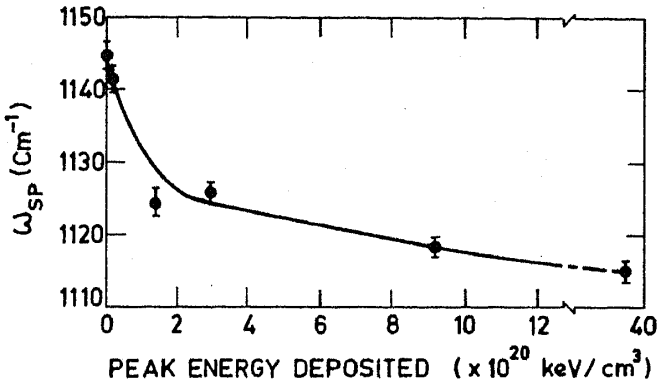

Figure 8. Variation with dose of one of the surface polariton frequencies of α-quartz following D^+ irradiation. Observe the similarity to figure 1.

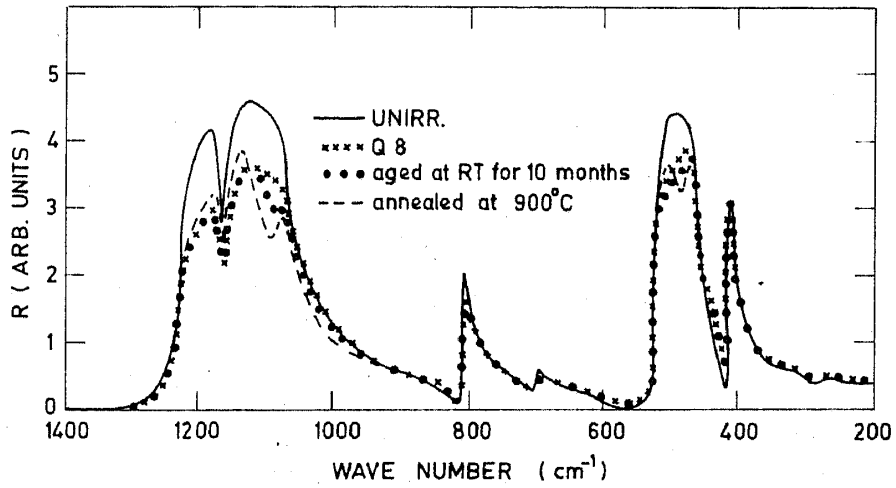

Figure 9. BR spectra for specimen Q8 (Ar^+ irradiated) immediately after irradiation and after various post-irradiation treatments. Observe that both room temperature ageing and annealing at 900°C assist recovery. However, the recovery is not complete.

ageing were found in the samples irradiated with D^+ or He^+, we confined our studies to samples irradiated with argon ions.

The specimens Q7 and Q8 (table 1) were annealed for 1 hr at various temperatures up to 900°C, and the BR and ATR spectra recorded. After every anneal, the specimen was quenched to room temperature for recording the spectra. Such time-temperature profiles are not unusual (*e.g.* Bates *et al* 1974; Martin *et al* 1982; Aguilar *et al* 1982). The annealing time of 1 hr was considered adequate since in practice the spectra saturated within 30 min at any given temperature. From various annealing studies performed earlier (especially in NaCl), we find that the saturation value $P(\infty; T)$ of a property P at temperature T does not depend on earlier thermal history, provided the sample has not been exposed earlier to a temperature *higher* than T. Indeed this idea is also tacitly implied by other workers who used a similar annealing procedure.

Figure 9 shows the BR spectra for specimen Q8 before irradiation, after irradiation, after ageing at room temperature for about 10 months and after annealing at 900°C for 1 hr. In figure 10 is shown the annealing behaviour for the surface polariton of (nominal) frequency 1125 cm^{-1} as observed with samples Q7 and Q8. One notices that

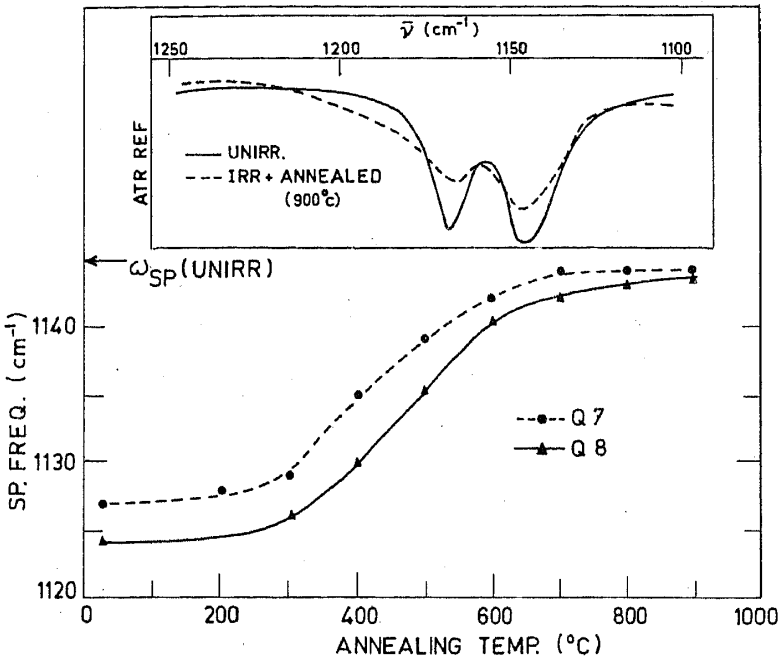

Figure 10. Annealing behaviour of the surface polariton of (nominal) frequency 1125 cm^{-1} as observed in samples Q7 and Q8. The inset compares the ATR spectrum after annealing with that of the unirradiated sample. While frequency recovery is complete, the shape recovery is not. A two-layer model is discussed in text (§5.2) which suggests that after annealing, the damaged layer resembles unirradiated fused quartz.

around 900°C there is a saturation. It is noteworthy that on completion of annealing, the spectrum does *not* recover back to that for the unirradiated specimen. We comment on this in the following section. For the present we also remark that our observations relating to room temperature ageing are somewhat similar to the recent results on room temperature ageing effects on blistering and surface roughening after Ar^+ bombardment of Mo single crystals (Kamada *et al* 1978) and of metallic glasses (Tyagi *et al* 1983).

4.4 *Fused quartz*

We now turn to FQ, results for which are presented in figures 11 and 12. As in α-quartz, there is an overall reduction in the reflectivity following irradiation, and also some changes in the BR spectrum, notably in the ranges 1300–950 cm^{-1} and 500–400 cm^{-1}. As regards surface polaritons, of the three at 1138, 485 and 402 cm^{-1} in the unirradiated specimen, only the first one shifts to lower frequencies and broadens on irradiation.

The argon-irradiated specimens FQ 14 and FQ 15 were subjected to heat treatment in the range 300–1200°C in steps of 50°C. The reflectivity spectrum for FQ 15 annealed to 500°C is shown in figure 13 along with the spectra obtained before and after irradiation. As may be seen, there is recovery following annealing treatment. Changes due to irradiation anneal out completely around 700°C. Also argon ion implantation does not facilitate surface crystallization at lower temperatures, in contrast to lithium implantation (Arnold 1980).

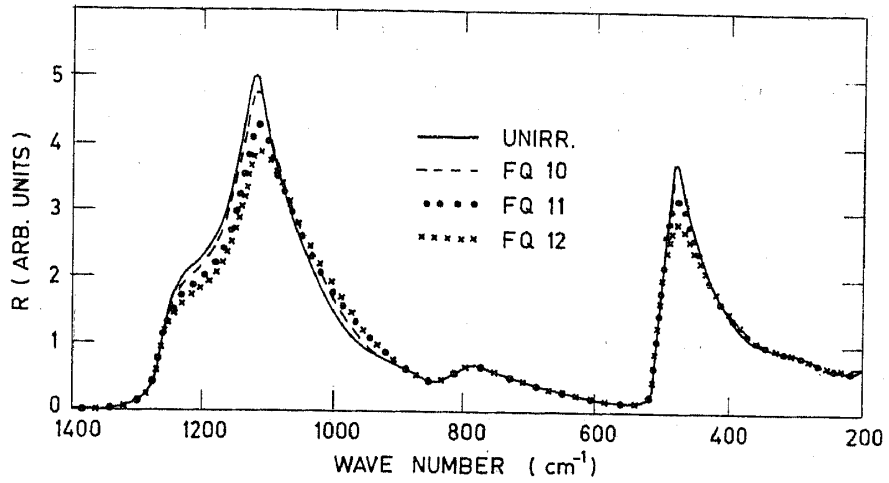

Figure 11. Typical (unpolarized) BR spectra for FQ.

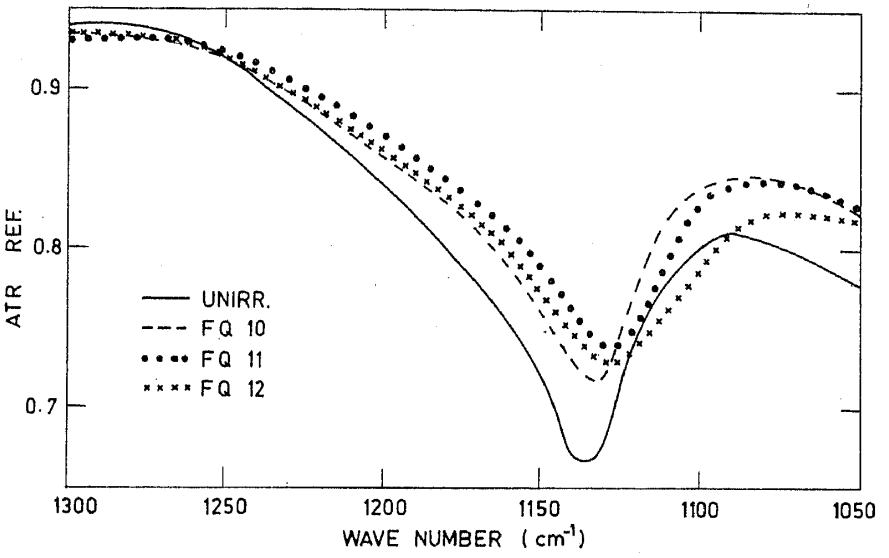

Figure 12. Typical ATR spectra for FQ in the range 1300–1050 cm^{-1}.

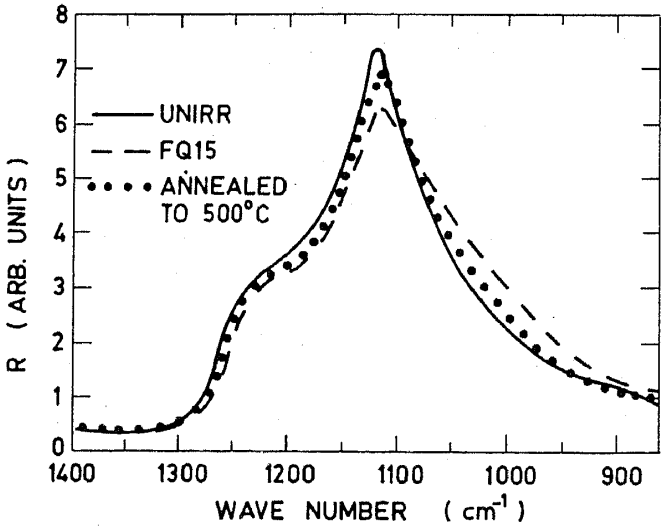

Figure 13. BR spectra for a representative FQ sample after irradiation and after post-irradiation annealing. For comparison, the spectrum for the unirradiated sample is also shown.

5. Analysis

We consider here the analysis and explanation of the observations. The basic facts to be explained are: (i) the changes produced by the irradiation, and (ii) the annealing behaviour.

5.1 *KK analysis of α-quartz*

The standard mode of analysis of IR data is through the well-known Kramer-Kronig (KK) relations. We have carried out such a KK analysis (using the computer program of Chandrasekar *et al* 1978). Representative plots for $\varepsilon_2(\omega)$ the imaginary part of the dielectric function $\varepsilon(\omega)$ obtained thus for the *E*-modes are given in figure 14. Also presented are some plots of the energy-loss function $\mathrm{Im}[-1/\varepsilon(\omega)]$.

One use of the KK analysis is that it provides the necessary inputs for the calculation of surface polariton spectra (Zhizhin *et al* 1979). The calculated frequencies for α-quartz are summarized in table 2, and are within 1–2% of those measured, a fact which gives confidence in the KK results.

5.2 *Two-layer model for α-quartz*

While the KK analysis no doubt leads to reasonable agreement as far as surface polaritons are concerned, the fact remains that an assumption has implicitly been made that the reflecting region is homogeneous. On the other hand, from figure 2 we know that there is a damaged surface layer and that the optical penetration depth ($= \lambda/(4\pi\kappa)$ where λ is the wavelength and κ the extinction coefficient) encompasses both the damaged and the undamaged regions. The optical radiation therefore sees an inhomogeneous material.

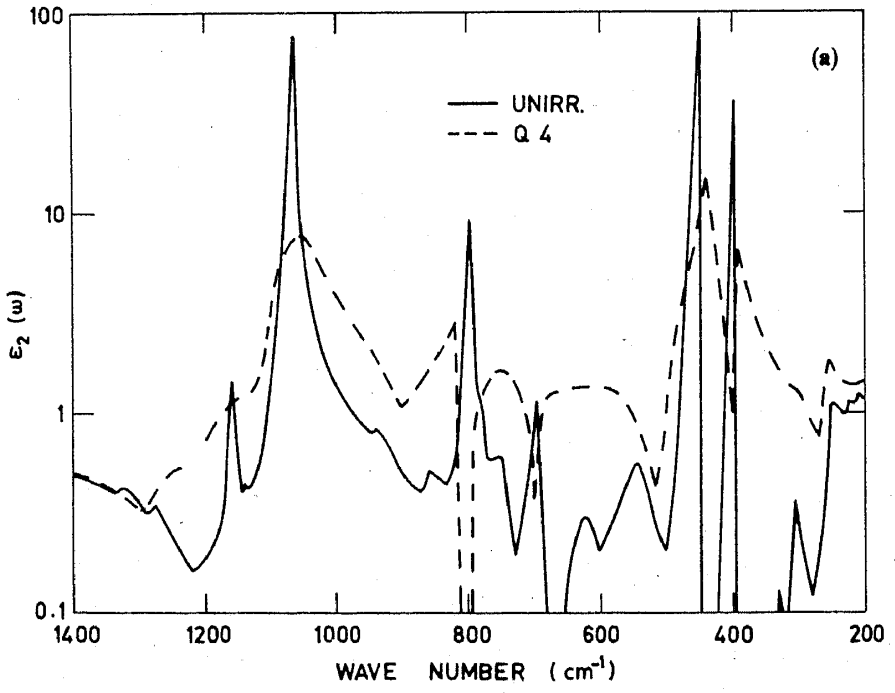

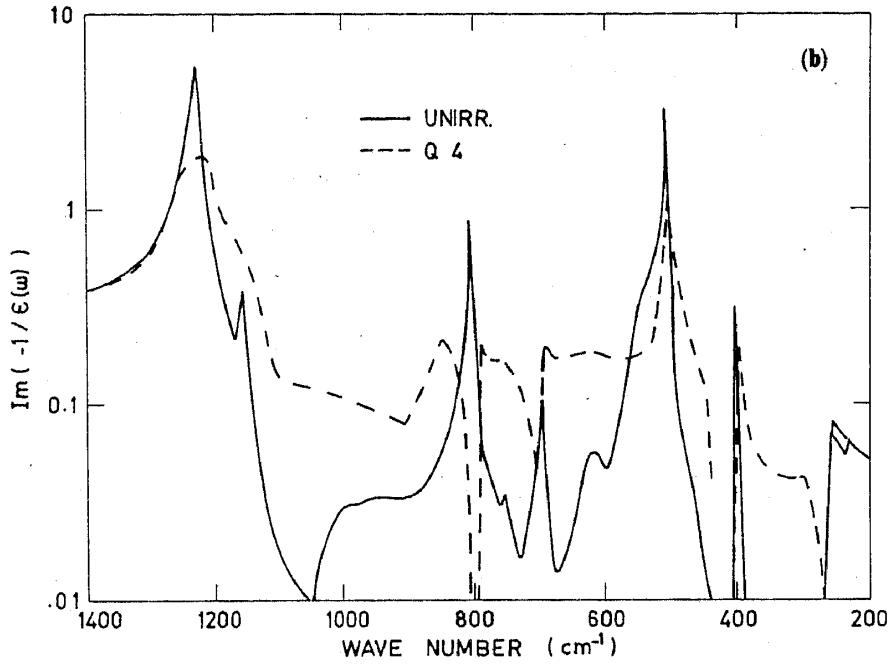

Figure 14. Representative results of the KK-analysis of α-quartz. **a.** shows typical plots of $\varepsilon_2(\omega)$, the imaginary part of the dielectric function. **b.** depicts some plots for the energy-loss function.

A simple model for such an inhomogeneity is a two-layer model in which the top layer represents the damaged material, and has a thickness t dictated by the damaged profile, while the layer beneath or the 'substrate' represents the undamaged material. One now ascribes different optical properties to the two layers, and calculates the reflectivity by classical dispersion formula.

We consider now such a model to explain our observations in irradiated α-quartz. The reflectivity R for a two layer reflector subjected to normal incidence is known to be given by (Heavens 1964)

$$R = \left| \frac{r_1 + r_2 \exp(2i\delta)}{1 + r_1 r_2 \exp(2i\delta)} \right|^2, \tag{1}$$

where r_1 and r_2 are the reflectance of the two layers. In our case they would be given respectively by

$$r_1 = \frac{(\varepsilon_{\text{irr}})^{1/2} - 1}{(\varepsilon_{\text{irr}})^{1/2} + 1}, \tag{2}$$

and

$$r_2 = \frac{(\varepsilon_{\text{unirr}})^{1/2} - (\varepsilon_{\text{irr}})^{1/2}}{(\varepsilon_{\text{unirr}})^{1/2} + (\varepsilon_{\text{irr}})^{1/2}}. \tag{3}$$

The phase δ is given by

$$= (2\pi/\lambda)(\varepsilon_{\text{irr}})^{1/2} t. \tag{4}$$

The dielectric functions ε_{irr} and $\varepsilon_{\text{unirr}}$ characterize the two layers, and we now have to specify them. Of these, the latter is obtainable from our own data for the unirradiated crystal. To extract the required dielectric function, we write (Gervais 1974)

$$\varepsilon(\omega) = \varepsilon_\infty \prod_j \frac{\omega_{LO}^2(j) - \omega^2 - i\gamma_{LO}(j)}{\omega_{TO}^2(j) - \omega^2 - i\gamma_{TO}(j)}. \tag{5}$$

The various quantities appearing on the right have their familiar meanings. In the spectral range scanned by us, there are seven E-modes (-the eighth one at $\sim 137\ cm^{-1}$ falls outside our range) and four A_2-modes. The reflectivity data for unirradiated α-quartz was accordingly fitted to a seven-oscillator formula to obtain ε_{unirr}. The oscillator strengths ρ_i defined by

$$\varepsilon(0) = \varepsilon_\infty + \sum_i 4\pi\rho_i \tag{6a}$$

were computed using

$$\rho_i = (1/2\pi^2) \int_{\text{ith band}} [\varepsilon_2(\omega)/\omega]\, d\omega. \tag{6b}$$

The parameters of the fit are listed in table 3, and agree with those reported earlier (Gervais and Piriou 1975).

Turning to $\varepsilon_{irr}(\omega)$, it is tempting to model it with the dielectric function for fused quartz on the assumption that irradiation leads to some vitrification of the damaged layer. Guided by earlier work (Taylor *et al* 1970; Mitchell *et al* 1972), we first made a nonlinear least squares fit of our data for unirradiated fused quartz to a three-oscillator model (using the VBO1A program of the Harwell Mathematical Library). The quality of the fit can be judged by reference to figure 15. The parameters obtained are listed in table 3.

With the inputs for the two layers available, we next fitted the data for Q4 (using the VBO1A program). Various values of the thickness t were tried. For each t value, the parameters for the top layer were regarded as free and those for (unirradiated) fused quartz were treated as *initial choice*. The best fit was judged on the basis of least squares and is shown in figure 16. The fit was achieved for $t = 1{\cdot}1\ \mu m$. The *final* parameters for

Table 3. Parameters from classical dispersion analysis.

Sample	ω_{LO} (cm^{-1})	γ_{LO} (cm^{-1})	ω_{TO} (cm^{-1})	γ_{TO} (cm^{-1})	Oscillator strength	ε_∞	$\varepsilon(0)$
Unirradiated	1226	12·5	1065	7·2	0·052		
α-quartz	1155	9·3	1158	9·3	0·0008		
	810	6·9	797	6·9	0·0088		
	697·6	13	695	13	0·0016	2·6	4·58
	510	4·1	450	4·5	0·066		
	402	2·8	393·5	2·8	0·026		
	267	30	265	30	0·0024		
Unirradiated	1268·8	142	1087·5	21·6	0·059		
fused quartz	812	28	807	28	0·0032	2·19	3·76
	507·5	12·6	454·7	24·3	0·063		
Top layer in	1255·3	144·5	1072	47	0·059		
the two-layer	857·9	50·2	854·6	63	0·0024	2·19	4·11
model	527·4	56·5	452·5	47·2	0·092		

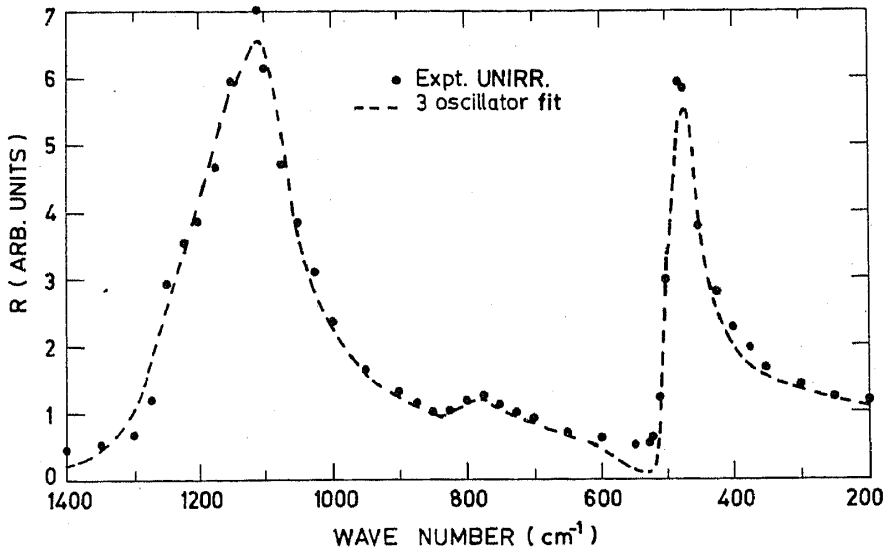

Figure 15. BR spectrum of unirradiated FQ as observed and as fitted by a three-oscillator formula. This fit was made to generate inputs for the two-layer model discussed in §5.2.

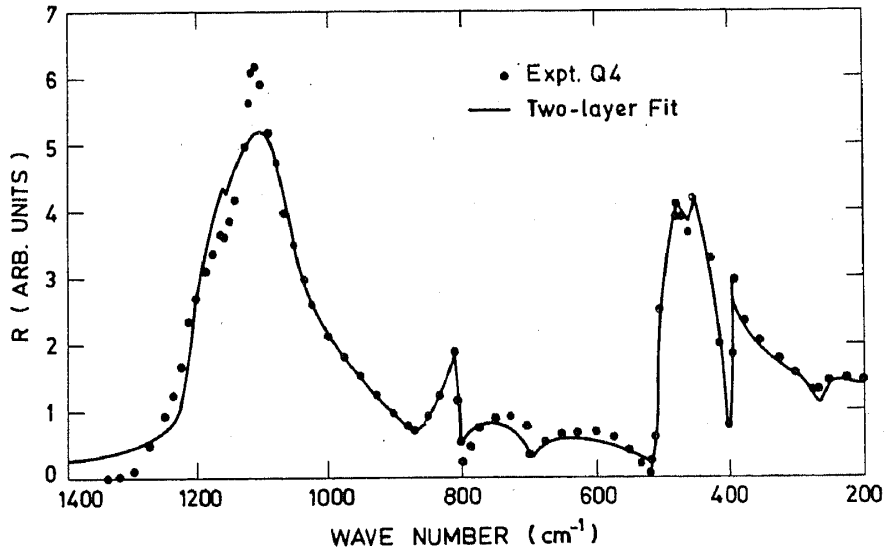

Figure 16. BR spectrum for irradiated α-quartz as observed and as fitted by the two-layer model. The damaged layer was treated as describable by three oscillators, initial parameters for which were taken from the results of figure 15. Note the reflectivity scale is *not* the same as in figure 4.

the *top* (*i.e.* irradiated) layer are listed in table 3. It is significant that the parameters that actually fit the observations are slightly different from those for unirradiated fused quartz suggesting that while irradiation no doubt produces amorphisation, the disorder is probably not quite the same as exists in fused quartz.

The data obtained from the above dispersion analysis was used to compute the surface polariton frequencies (see Appendix), and the results are given in table 2.

Directing attention now to the annealing studies on argon-irradiated α-quartz, we recall from §4 that while annealing no doubt produces some recovery, the BR spectrum

of the fully annealed sample still does not match with that of the unirradiated sample. This suggests that recovery is partial and not complete. Remembering the irradiation results for fused quartz (see figure 13) wherein a distinct difference is observed in the spectra for irradiated and unirradiated material, we speculated that perhaps an amorphous top layer still survived in the annealed specimen which was characteristic of *unirradiated* FQ rather than *irradiated* FQ. To test this hypothesis, calculations were performed using the two-layer model, with the top layer characterized by parameters appropriate to (i) irradiated (alpha) quartz (*i.e.* the parameters listed in table 3 and obtained *via* the fit to the two-layer model described earlier), and (ii) unirradiated FQ. The parameter t was varied as before, and the value that yielded the least residual square was determined. The values for the two cases referred to above are respectively 0·08 μm and 0·14 μm. The results of the two calculations are displayed in figure 17. It must be stressed that each of the two graphs in figure 17 is not very sensitive to the t value chosen, on the scale in which the results are displayed. The pronounced dip near 1085 cm^{-1} for model (ii) is just not produced by model (i). Comparison with experiment (see figure 9) shows the superiority of model (ii). In particular, the experimentally observed dip at 1085 cm^{-1} is reproduced.

It thus seems that after the annealing, there is still some residual amorphization in the top layer but characteristic of *unirradiated* FQ. It is also noteworthy that in FQ, there is complete recovery of damage following annealing treatment (see figure 13). In effect, post irradiation annealing of α-quartz produces a recovery in the direction of FQ rather than crystalline quartz.

The annealing behaviour observed is quite interesting, and obviously a detailed explanation must necessarily be linked to the structural details. At present this is not fully possible. However, the recent work of Nelson (1983) on defects in glasses might perhaps offer some clue, although his focus is primarily on metallic glasses. Studying

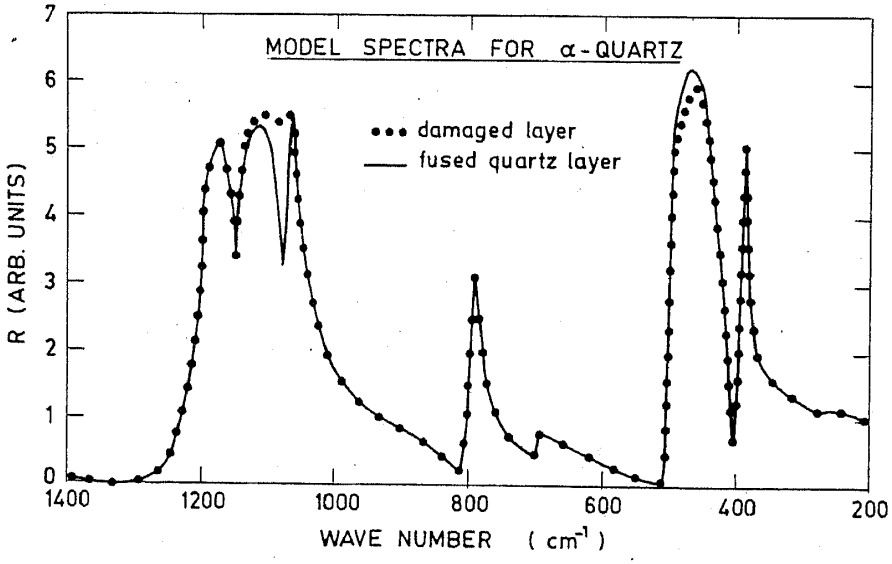

Figure 17. Results of further calculations based on the two-layer model to elucidate the nature of the spectrum observed in the annealed sample of α-quartz. The two spectra shown here are based on two different assumptions for the top (*i.e* damaged) layer as discussed in text. Comparison of these computed curves with experiment (figure 9) suggests that after annealing, the top-layer resembles unirradiated FQ.

the average coordination number Z and the average number of tetrahedra q packed around a bond, Nelson finds from a plot of Z *vs* q that there is a hierarchy *viz.*: liquid, unrelaxed dense random packing, relaxed dense random packing and finally the crystalline phase. Presumably a similar hierarchy exists in the present systems also. In that case, one visualizes that radiation essentially produces an unrelaxed random structure while annealing takes it back only up to the relaxed random structure. Such a picture is qualitatively consistent with our observations.

5.3 KK *analysis of* FQ

The KK analysis for FQ has already been discussed briefly in the context of the two-layer model. Here we pursue that subject to understand the changes in FQ caused by irradiation.

In crystals, the peaks in $\varepsilon_2(\omega)$ and the energy-loss function $\mathrm{Im}\,[-1/\varepsilon(\omega)]$ correspond to the TO and LO modes respectively. KK analysis for FQ reveals peaks, indicating the presence of characteristic vibrational modes, although one may not strictly be able to label them as TO or LO (Galeener and Lucovsky 1976). The frequencies emerging from our analysis are given in table 4, where the full widths at half maximum of the peaks are also quoted. The observed bandshapes are not symmetrical, an explanation for which has earlier been given by Gaskell and Johnson (1976).

Our interest is in extracting a measure which will give some idea of the structure change caused by radiation. For this purpose, we appeal first to a central force model of atomic vibrations as applied to a continuous random network. In this model, every silicon atom bonds tetrahedrally to four oxygen atoms and every oxygen atom bridges two silicon atoms. If α is the Si-O stretching force constant and θ the inter-tetrahedral Si-O-Si angle, then (Galeener 1979)

$$\alpha = \tfrac{1}{2}(\omega_3^2+\omega_4^2)M_0(1+4M_0/3M_{\mathrm{Si}})^{-1}, \tag{7}$$

$$\cos\theta = (\omega_3^2-\omega_4^2)(\omega_3^2+\omega_4^2)^{-1}(1+4M_0/3M_{\mathrm{Si}}). \tag{8}$$

Here M_0 and M_{Si} are the masses of oxygen and silicon atoms respectively, and ω_3, ω_4 are the frequencies of the high frequency modes (*i.e.* $\sim 800\ \mathrm{cm}^{-1}$ and $1200\ \mathrm{cm}^{-1}$). The central-force assumption is obviously inadequate for a covalently-bonded system like quartz. Galeener (1979) has therefore argued for the inclusion of a noncentral force constant β such that

$$\beta \sim \tfrac{1}{2}\omega_0^2 M_0, \tag{9}$$

where ω_0 is the frequency of the TO mode (and is $450\ \mathrm{cm}^{-1}$ in the present case). With such a model, Galeener (1979) obtained agreement with the large cluster calculations of Bell *et al* (1970).

Assigning to ω_0, ω_3 and ω_4 the various values as noted in table 4, we have calculated α, θ and β for the model discussed (see table 5). Now Galeener has also used the model to estimate the spread in θ from the observed width of the spectral line. Using the width $\Delta\omega_{\mathrm{TO}}$ observed by us for the TO mode near $1080\ \mathrm{cm}^{-1}$, we estimate $\Delta\theta$ using the expression

$$\Delta\theta = \frac{2\omega_{\mathrm{TO}}\,\Delta\omega_{\mathrm{TO}}\,M_0}{\alpha\sin\theta} \tag{10}$$

(see table 5). One observes that upon irradiation, which is a measure of disorder,

Table 4. Parameters for fused quartz from KK analysis.

Sample	ω_{LO} (cm^{-1})	FWHM of LO mode (cm^{-1})	ω_{TO} (cm^{-1})	FWHM of TO MODE (cm^{-1}) ($\omega_h - \omega_l$)	Asymmetry ($\omega_h - \omega_{TO}$)	Asymmetry ($\omega_l - \omega_{TO}$)
Unirradiated	1261 (ω_4)	56	1078	70	25	45
	817 (ω_3)	67	797	65	42	23
	504	25	455 (ω_0)	38	15	25
FQ12	1256 (ω_4)	69	1045	109	53	56
	827 (ω_3)	113	810	121	75	46
	504	28	444 (ω_0)	57	24	33

Remarks: In the above, ω_{LO} and ω_{TO} refer to the peak frequencies, ω_h and ω_l refer to the frequencies corresponding to half maximum on the high and low side respectively of the peak frequency.

Table 5. Analysis for fused quartz using Galeener's (1979) model.

Sample	α (N/m)	β (N/m)	θ (degrees)	$\Delta\theta$ (degrees)
Unirradiated	604·8	98	136	19·3
FQ12	606·5	93·3	134	28·2

increases from ~ 19·3° to 28·2°, representing an increase of ~ 47%. A similar trend has been noted earlier in small-angle x-ray measurements on neutron irradiated quartz (Bates *et al* 1974).

It has been suggested that changes in density caused by irradiation result from maximization of π-bonding character (Revesz 1972). Such a redistribution of electron density has implications for the effective charge carried by the ions. In principle, changes in vibrational frequencies should offer some clue about changes in the effective charge. As a rough check, we used the following relation (Scott 1971; Gervais and Servoin 1981)

$$\sum_j \{\omega_{LO}^2(j) - \omega_{TO}^2(j)\} = (1/\varepsilon_v V)\sum_k (Z_k^2/M_k), \tag{11}$$

where V is the unit cell volume, Z_k the (rigid-ion) effective charge (Venkataraman *et al* 1975) of the kth ion in the unit cell, M_k its mass, and ε_v the dielectric constant of vacuum. The sum

$$Y \equiv \sum_{j=1}^{3} \{\omega_{LO}^2(j) - \omega_{TO}^2(j)\}$$

was computed for FQ and FQ12 from the observed frequencies. A 12% increase in Y was found in going from the unirradiated to the irradiated sample. Based on (11), this increase in Y is suggestive of changes in the effective charge. However, a more careful study is required to make a qualitative assessment.

6. Summary and conclusions

α-quartz and FQ have been irradiated with low energy (~ 100keV)D^+, He^+ and Ar^+ ions, and the changes in the optical properties in the IR region have been studied by measuring the BR and ATR spectra. Unlike neutron irradiation, ion irradiation produces only surface damage. In this respect, ATR studies are useful since they probe the surface *via* surface polariton frequencies. (However, it must be remembered that the optical penetration depth encompasses to some extent the undamaged region also.)

From the damage profiles (figure 2) one sees the big difference in the range for deuterium and argon ions. This, together with the differences in sputtering yield, leads to significant differences in the post irradiation spectra (figures 3 and 4), even though the fluence might be the same. By varying the fluence, one can change the deposited energy density, and the variation of the frequency of one of the surface polaritons in α-quartz as a function of the deposited energy density reveals a trend very similar to that observed earlier (Gotz 1981) for the *refractive index* (compare figures 1 and 8). The refractive index variation has been previously correlated (Brueckner 1971; Revesz 1972) to radiation-induced density changes. One can now say that the changes in the optical properties as studied in the visible and the IR regions arise from the same basic cause namely, reorganization of the atomic structure following irradiation.

There is already evidence from neutron irradiation of α-quartz that irradiation produces structural disorder bordering on amorphization. Our results also suggest the same although it must be admitted that unlike in neutron irradiation where there is bulk damage, ion bombardment produces only surface damage. In the context of amorphization produced by irradiation, it is significant that fused quartz when irradiated, also shows changes.

One expects that annealing will promote the recovery of damage. One observes this in argon-irradiated samples but not so much in deuteron-irradiated samples. Presumably the lower range and greater sputtering yield for argon facilitate annealing.

Annealing studies on argon-irradiated samples show that whereas in FQ there is complete recovery, in α-quartz there is, even after annealing, a residual disorder. Analysis *via* a two-layer model suggests that the residual disorder resembles *unirradiated FQ*. Thus the recovery of the amorphous region created by irradiation appears to be in the direction of FQ rather than crystalline quartz. A qualitative understanding of this trend is possible by analogy with observations made by Nelson (1983) in the case of metallic glass.

Our broad aim has been to understand the structural changes (in quartz) caused by irradiation. In the ultimate analysis of course atomic structure is intimately linked to electronic structure. In the context of structure changes in quartz, there has been some speculation (Revesz 1972) that density changes are linked to changes in the π-bonding character. This in turn has implications for the effective charge carried by the ions. Our studies suggest that there is quite likely a change in the effective charge. However, more detailed experiments are needed to establish this quantitatively.

Acknowledgements

The authors are grateful to S Panchapakesan for assistance with the irradiation. H K Sahu collaborated in the initial stages of the experiment.

Appendix

We briefly outline here how we computed the ATR spectrum, and estimated from it the surface polariton frequencies.

The attenuated total reflectivity $R_{AT}(\omega)$ is a composite effect involving several media and interfaces. In unirradiated samples, one has three regions $i = 1, 2, 3$ *viz*, the ATR prism, the air gap and the specimen itself. In irradiated samples, i runs from 1 to 4, with $i = 3$ now representing the damaged layer and $i = 4$ representing undamaged material.

Define now:

$$\beta_i = x_i/\varepsilon(\omega; i),$$

with

$$x_1 = [\varepsilon(\omega; 1)]^{1/2} \cos\theta,$$

where θ is the angle of incidence in the ATR prism, and

$$x_n = \{\varepsilon(\omega; 1)\sin^2\theta - \varepsilon(\omega; n)\}^{1/2}$$

with $n = 2, 3$ for 1-layer ATR and $n = 2, 3, 4$ for 2-layer ATR.

$R_{AT}\omega$ can now be expressed in terms of the above quantities. One has (Mirlin and Reshina 1975; Bryskin *et al* 1972)

$$R_{AT}(\omega) = |[1 + iP(\omega)]/[1 - iP(\omega)]|^2,$$

where

$$P(\omega) = \tfrac{1}{2}\left(\frac{1 + A_2 \exp(-2x_2\omega d/c)}{1 - A_2 \exp(-2x_2\omega d/c)}\right)$$

with

$$A_2 = \frac{(\beta_2 - \beta_3) + A_3(\beta_2 + \beta_3)}{(\beta_2 + \beta_3) + A_3(\beta_2 - \beta_3)},$$

$$A_2 = 0 \quad \text{for 1-layer ATR}$$

$$= [(\beta_3 - \beta_4)/(\beta_3 + \beta_4)]\exp(-2x_3\omega t/c) \quad \text{for 2-layer ATR.}$$

In the above, d is the thickness of the air gap and t is thickness of the damaged layer.

Given $\varepsilon(\omega; i)$, $R_{AT}(\omega)$ can be computed using the above expressions. Dips in $R_{AT}(\omega)$ are identified as surface polaritons.

References

Aguilar G M, Rubio O J, Lopez F J, Garcia-Sole J and Murrieta S H 1982 *Solid State Commun.* **44** 141
Arnold G W 1980 *Radiat. Eff.* **47** 15
Bates J B, Hendricks R W and Shaffer L B 1974 *J. Chem. Phys.* **61** 4163
Bayly A R 1973 *Radiat. Eff.* **18** 111
Bell R J, Dean P and Hibbins-Butler D C 1970 *J. Phys.* **C3** 2111
Brueckner R 1971 *J. Non-Crys. Solids* **5** 123
Bryksin V V, Gerbshtein Yu M and Mirlin D N 1972 *Sov. Phys. Solid State* **14** 453
Chandrasekhar H R, Burns G and Chandrasekhar G V 1978 *Solid State Commun.* **27** 829
Gaskell P H and Johnson D W 1976 *J. Non-Cryst. Solids* **20** 153
Galeener F L and Lucovsky F 1976 *Phys. Rev. Lett.* **37** 1474
Galeener F L 1979 *Phys. Rev.* **B19** 4292

Gervais F 1974 *J. Phys.* **C7** 2374
Gervais F and Piriou B 1975 *Phys. Rev.* **B11** 3944
Gervais F and Servoin J L 1981 *J. Phys. (France)* **C6** 415
Gotz 1981 *Proc. Int. Conf. on Amorphous Systems Investigated by Nuclear Methods* (Balantonfured, Hungary) Vol. 1 151
Grasse D, Kocar O, Pesol H, Moss S C and Golding B 1981 *Phys. Rev. Lett.* **46** 261
Heavens O S 1964 *Optical properties of thin films* (London: Butterworth) 76
Hines R L and Arndt R 1960 *Phys. Rev.* **119** 623
Kamada K, Naramoto H and Kazumata Y 1978 *J. Nucl. Mater.* **71** 249
Karge H and Prager R 1976 *Exp. Tech. Phys.* **24** 87
Manning I and Mueller G P 1974 *Comp. Phys. Commun.* **7** 85
Martin J J, Harness V J, Orozco E M, Mendoza A A and Rubio O J 1982 *Philos. Mag.* **A46** 269
Mirlin D L and Reshina I I 1975 *Sov. Phys. Solid State* **16** 1463
Mitchell D L, Bishop S G and Taylor P C 1972 *J. Non-Cryst. Solids* **8** 231
Nandedkar R V 1981 *Radiation damage studies in nickel-based crystalline and amorphous alloys* Ph.D. Thesis, Indian Institute of Science, Bangalore
Nelson D R 1983 *Phys. Rev.* **B28** 5514
Otto A 1968 *Z. Phys.* **216** 398
Presby H M and Brown W L 1976 *Appl. Phys. Lett.* **24** 87
Primak W and Kampwirth R 1968 *J. Appl. Phys.* **39** 5651
Primak W 1975 *The compacted states of viterous silica* (New York: Gordon and Breach)
Primak W 1976 *Phys. Rev.* **14** 4679
Revesz A G 1972 *Solid State Commun.* **10** 127
Schineller E R, Flarn R P and Wilmat 1968 *J. Opt. Soc. Am.* **58** 1171
Scott J F and Porto S P S 1967 *Phys. Rev.* **161** 903
Scott J F 1971 *Phys. Rev.* **B4** 1360
Sigmund P 1969 *Phys. Rev.* **184** 383
Taylor P C, Bishop S G and Mitchell D L 1970 *Solid State Commun.* **8** 1783
Tyagi A K, Nandedkar R V and Krishan K 1983 (Private communication)
Umadevi V, Kesavamoorthy R and Sood A K 1980 *Proc. Nucl. and Solid State Phys. India* **C23** 701
Venkataraman G, Feldkamp L A and Sahni V C 1975 *Dynamics of perfect crystals* (Cambridge, Mass. MIT Press).
Webb A P and Townsend P D 1976 *J. Phys.* **D9** 1343
Zhizhin G N, Yakovlev V A and Shirmer G 1979 *JETP Lett.* **29** 315